Neuron, Vol. 19, 1319–1327, December, 1997, Copyright ©1997 by Cell Press

Voltage-Dependent Proton Transport by the Voltage Sensor of the *Shaker* K^+ Channel

Dorine M. Starace,* Enrico Stefani,*† and Francisco Bezanilla*‡
*Departments of Physiology and Anesthesiology
UCLA School of Medicine
Los Angeles, California 90095
†CONICET
Buenos Aires
Argentina

Summary

In voltage-dependent ion channels, pore opening is initiated by electrically driven movements of charged residues, and this movement generates a gating current. To examine structural rearrangements in the *Shaker* K^+ channel, basic residues R365 and R368 in the S4 segment were replaced with histidine, and gating currents were recorded. Changes in gating charge displacement with solvent pH reveal voltage-dependent changes in exposure of the histidine to solvent protons. This technique directly monitors accessibility changes during gating, probes the environment even in confined locations, and introduces minimal interference of gating charge motion. The results indicate that charges 365 and 368 traverse the entire electric field during gating. The remarkable implication of the successive exposure of histidine to each side of the membrane is that in a pH gradient, the voltage sensor transports protons.

Introduction

The propagation of an action potential in nerve cells is the result of an exquisite regulation of pore opening in potassium and sodium channels by the transmembrane potential (Hodgkin and Huxley, 1952). The voltage dependence of pore opening arises from an electrically driven movement of charged residues in the channel, and this movement generates a gating current preceding the ionic current (Armstrong and Bezanilla, 1973). The process of voltage gating has been most thoroughly characterized in the cloned *Shaker* K^+ channel, since it expresses abundantly in Xenopus laevis oocytes, and conduction can be abolished by a pore mutation without affecting gating (Perozo et al., 1993). The *Shaker* K^+ channel consists of four identical subunits (MacKinnon, 1991), each of which has six putative membrane-spanning segments (S1–S6) (Figure 1). Three basic residues, R365, R368, and R371, in S4 and the acidic residue E293 in S2 contribute charge to the gating current (Aggarwal and MacKinnon, 1996; Seoh et al., 1996). It is significant that although seven positive residues span S4, only the central three are the main contributors to the gating current. The other charges either are exposed to the solvent and therefore are outside the electric field or do not move in the field. Ultimately, an understanding of gating charge movement and how it couples to channel opening requires characterization of both the conformational changes that occur and the local electric field that determines charge movement.

Examination of the accessibility of specific residues to probes in the bulk solvent as a function of the state of the channel provides information about how the local environment changes with channel gating. By determining if membrane-impermeant thiol probes could label cysteines substituting residues in S4, a central region not exposed to the surrounding solvent has been outlined, and the boundaries of this buried region are different in the closed and open states of the channel (Larsson et al., 1996; Yusaf et al., 1996). Similar experiments have been reported for a voltage-gated Na^+ channel (Yang and Horn, 1995; Yang et al., 1996). Although valuable insights to the mechanism of gating charge motion have been gained with site-directed labeling of substituted cysteines, resolution of confined spaces is limited by the large size of the thiol probe, and the movement and charge of the original residue may be significantly disturbed by cysteine substitution and probe attachment.

To examine the environment of charged residues with minimal perturbation and high resolution, the voltage-sensing residue R365 or R368 was replaced with histidine, and the charge of the histidine was measured as part of the gating currents. If the histidine becomes exposed to the bulk solution, its charge can be modified by the bulk pH; consequently, the gating charge transported upon membrane voltage changes will be affected and observed in the gating currents. The small size of the proton probe offers the advantages of access to spaces in the protein too restricted for larger cysteine probes and minimal interference of residue size and motion. Furthermore, contact of the histidine residue with the bulk solution on each side of the membrane in a state-dependent manner will result in a net transport of protons across the membrane under a pH gradient, as the residue successively samples both sides during its motion.

Results

Individual histidine substitutions were performed on a nonconducting (W434F) (Perozo et al., 1993), noninactivating (IR, Δ6–46) (Hoshi et al., 1990) version of the *Shaker* H4 K^+ channel (Schwarz et al., 1988). The resulting channels, H4IR[W434F][R365H] and H4IR[W434F][R368H] will be referred to as the R365H and R368H channels, respectively. Gating currents in response to various test pulses from an extremely hyperpolarized potential (−130 mV) were measured with the cut-open oocyte voltage-clamp technique (Stefani et al., 1994); an on-gating current was evoked by the onset of a depolarizing test pulse and an off-gating current by the return to hyperpolarized potential. Gating charge displacement (Q) was determined by integrating the gating currents.

‡To whom correspondence should be addressed.

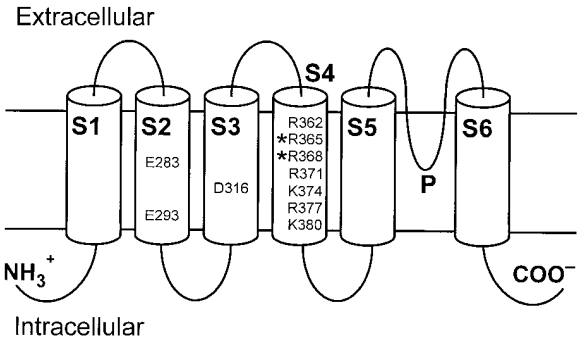

Figure 1. Conventional Model of the Topology of a *Shaker* K^+ Channel Subunit

Six transmembrane segments (S1–S6), the pore-forming region (P), and the location of charged residues in S2, S3, and S4 are shown. The residues replaced with histidine are marked with an asterisk.

Conductance of Protons Transported by Movement of the Histidine-Substituted Voltage Sensor

The on-gating currents of the R365H channel, recorded in pH 9.2 solutions on both sides of the membrane, are shown in Figure 2A. Accessibility studies with site-directed cysteine labeling have shown that residue 365 gets exposed to the external solution after one depolarizing pulse (Larsson et al., 1996). Upon exposure, it is most likely that the His-365 residue equilibrates with the external solution, since the rate constants for protonation and deprotonation of a His residue (Eigen et al., 1960; Kasianowicz et al., 1987) are much greater than those for transitions in gating (Bezanilla et al., 1994). Therefore, in symmetric pH 9.2, the His-365 residue was expected to be uncharged. As reported for the neutralization mutant H4IR[R365Q] (Seoh et al., 1996), the voltage dependence of gating charge displacement in the R365H channel in symmetric pH 9.2 was shifted to more hyperpolarized potentials relative to the wild-type channel, and charge movement saturated at a maximum value at −50 mV (Figure 2A). Otherwise, the gating currents exhibit the same general features as those of a wild-type channel (Perozo et al., 1993; Stefani et al., 1994); they are transient capacitive currents, and charge movement saturates with increasing driving potential. When a pH gradient was imposed across the membrane, the gating currents changed drastically. The on-gating currents recorded in external pH 5 and internal pH 9.2 solutions had a normal transient component, but at several potentials a steady inward current appeared (Figure 2B). The inward current increased as the membrane was increasingly depolarized, peaked at around −60 mV, and then decreased and became zero at very depolarized potentials. The range of voltage in which the steady current emerges is also the range in which gating charge movement is most steeply voltage-dependent. No pH-dependent steady current was observed in channels without the His-365 replacement (data not shown). The appearance of a steady current that flows down the pH gradient and is specific to a protonatable histidine suggests that it is a current of protons transported by the His-365 residue as it moves with the voltage sensor. If so, reversal of the transmembrane pH gradient should reverse the direction of the steady current from the R365H channel. The gating currents measured in external pH 9.2 and internal pH 7.4 are shown in Figure 2C. In these conditions, the direction of the steady current was outward, consistent with the transport of protons from the acidic internal solution to the basic external solution by the His residue. As with the inward proton current, the amplitude of the outward proton current is maximal near the voltage of half maximal gating charge displacement.

The R365H channel proton current is not driven by the transmembrane voltage in a linear relationship typical of ion conductance through a channel pore; rather, the relationship of the proton conductance with voltage resembles that between the gating capacitance (dQ/dV) and voltage. An isochronal plot of proton current amplitudes as a function of membrane potential is shown in

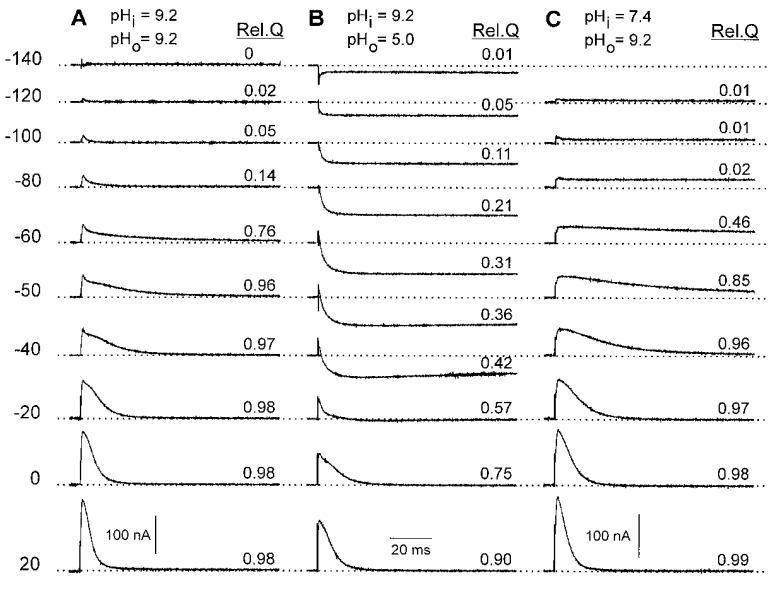

Figure 2. Transmembrane Proton Transport by the R365H Channel

On-gating currents in response to test pulses ranging from −140 to 20 mV, from an initial transmembrane potential of −130 mV, were measured in K^+- and Na^+-free isotonic solutions. The value of the test pulse evoking each gating current is shown to the left of the current traces. The fraction of the maximum gating charge displaced (Rel. Q, shown at the right of each trace) was obtained by integrating the transient component of the gating current over the duration of the test pulse and normalizing to the maximum value of the test pulse set. The direction of current is outward above the dashed baseline and inward below the baseline. All on-gating current traces were corrected as described in Figure 3.

(A) On-gating currents measured in internal and external solutions of pH 9.2 (pH_i/pH_o = 9.2/9.2).

(B) On-gating currents measured in pH_i/pH_o = 9.2/5.0.

(C) On-gating currents measured in pH_i/pH_o = 7.4/9.2.

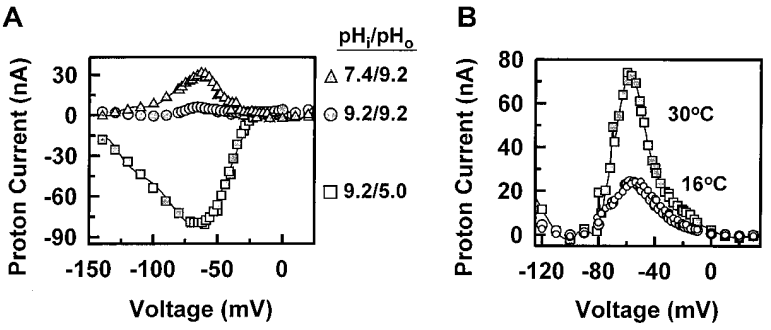

Figure 3. Voltage Dependence of Proton Transport by the R365H Channel

For each test pulse, the average value of the on-gating current over 5 ms and beginning at least 75 ms post-test pulse was determined. This group of isochronal current amplitudes was plotted as a function of voltage. The component that increased linearly with voltage (leak) was fit to a straight line and subtracted from the isochronal current at each potential to produce the proton current amplitudes; the same linear leak value was also subtracted from the on-gating currents shown in Figures 2 and 4A. Justification for this subtraction method was provided by measuring steady-state leak conductance in uninjected oocytes and in the H4IR[W434F] channel. In both cases, the leak current was linear with voltage up to about 10 mV, and leak conductance did not change with pH (data not shown).

(A) Voltage dependence of isochronal proton current amplitudes from the on-gating currents shown in Figure 2.

(B) Voltage dependence of isochronal proton current amplitudes obtained in pH$_i$/pH$_o$ = 5/8.1 from on-gating currents measured at 16°C before (closed circles) and after (open circles) measurement at 30°C (closed squares).

Figure 3A for each set of on-gating currents discussed above. In symmetric pH 9.2, the isochronal plot is close to zero at all potentials (Figure 3A, circles). The proton current elicited by application of a transmembrane pH gradient was in the same direction as the gradient, and, at the voltages where it was nonzero, the current amplitude was greater in the larger pH gradient (Figure 3A, triangles and squares). The isochronal plots of both the inward (squares) and outward (triangles) currents display that the maximum proton current occurred at −60 mV, near the voltage of half-maximal gating charge displacement (the midpoint of the Q-V curve, Figure 5C). At this voltage, it is equally probable that the voltage sensor occupies a hyperpolarized favored state or a depolarized favored state, so that the frequency of transitions between the two states is greatest. Since the His-365 residue transports protons across the membrane, it must continuously oscillate between exposure to the internal and external solutions with these transitions of the voltage sensor and thereby generates a sustained proton current. The size of the current increases with the frequency that the voltage sensor shuffles back and forth between states and approaches zero at very hyperpolarized or depolarized potentials as the transitions become more infrequent and the voltage sensor remains in one of the states. Therefore, in the presence of a pH gradient across the membrane, the His-substituted voltage sensor becomes a voltage-dependent proton transporter.

The correlation between the voltage of maximum proton current and the midpoint of the Q-V curve for gating and the similarity of the steepness of the voltage dependence for these two processes provide strong evidence that the proton transport is coupled to gating of the channel. Gating charge movement is steeply temperature-dependent, indicative of a process involving transitions across large energy barriers (Rodriguez et al., 1995). Gating currents of the R365H channel were measured at 30°C and 16°C in external pH 8.1 and internal pH 5 solutions. An isochronal plot of the proton current at these two temperatures is shown in Figure 3B. At the peak current, the temperature dependence of the proton current had a Q_{10} of 2.6, close to the Q_{10} of the kinetics of gating currents in the *Shaker* K^+ channel (Rodriguez et al., 1995). This agreement gives additional confirmation of a coupling between gating and proton transport. The alternatives, a voltage-dependent conduction of protons through the channel pore or through a channel endogenous to the oocyte, are unlikely since the Q_{10} of conduction through the *Shaker* K^+ channel is only 1.3 (B. M. Rodriguez et al., unpublished data) and since no proton current was observed in control experiments performed with the H4IR[W434F] channel (data not shown).

Replacement of the neighboring voltage-sensing residue Arg-368 with a histidine also transformed the voltage sensor into a proton transporter (Figure 4). The mechanism of transport as explained for R365H seems to be the same for the R368H channel; there is a coupling between titration of the His-368 residue and the movement of the voltage sensor that carries His-368 from the internal to the external solution in a voltage-dependent manner.

Titration of Gating Charge Movement in the R365H Channel

Proton transport requires protonation of the His-365 residue on one side of the membrane and deprotonation on the other. Since transport is coupled to gating, this change in charge of His-365 will produce a difference in the gating charge displaced in the outwardly moving on-gating current relative to the charge that returns in the off-gating current. There will be no such asymmetry in gating charge movement in the absence of a pH gradient when the His charge is the same on both sides of the membrane. Gating currents of the R365H channel, in response to a test pulse to 10 mV, recorded in internal pH 9.2 solution and various external pHs, are shown in Figure 5A. The increasing asymmetry in the gating charge motion with increasing pH gradient affirms that the charge of His-365 differs in the depolarized and hyperpolarized states. Exposure of His-365 to the external solution occurs in the depolarized state since the charge displaced in the off-gating currents can be titrated with external pH. Exposure to the internal solution occurs in the hyperpolarized state since the charge displaced in the on-gating currents remains relatively constant, regardless of the His-365 charge returning from the depolarized state.

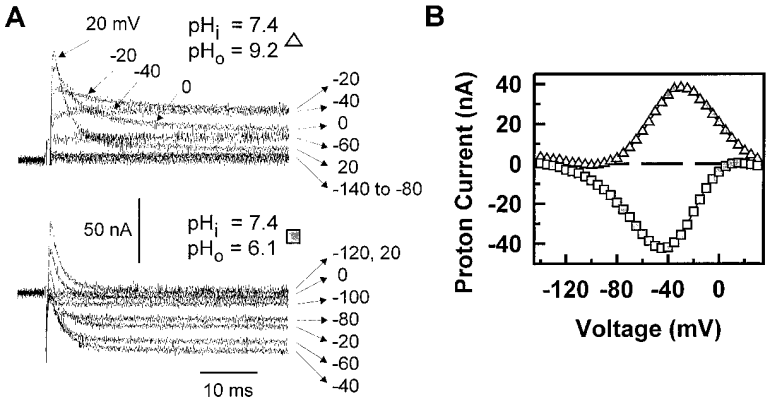

Figure 4. Proton Transport in the R368H Channel

(A) On-gating currents measured in pH_i/pH_o = 7.4/9.2 (top) and pH_i/pH_o = 7.4/6.1 (bottom). The current traces are shown superimposed for test pulses every 20 mV and are labeled with the potential of the test pulse. The current traces were corrected as described in Figure 3.

(B) Voltage dependence of isochronal proton current amplitudes from the on-gating currents shown in (A). The plots were determined as described in Figure 3.

The charge that the His-365 residue contributes to the gating current was determined by titrating the residue with external protons and measuring the displacement of gating charge. The voltage dependence of gating charge displacement (Q-V curve), generated by integrating the gating currents measured at a range of test potentials, was acquired for various external pHs while maintaining the internal pH at 9.2. When the external pH was changed from 9.2 to 5, the increase of charge displaced in the off-gating currents shows that the His residue is externally exposed and protonated in the depolarized states (Figure 5B). The Q-V relationship of on- and off-gating were the same in symmetric pH 9.2 conditions since protonation of His-365 was the same in hyperpolarized and depolarized states (Figure 5C; on, closed circles; off, open circles). Upon changing the external pH to 5, a pH gradient was established, and gating charge movement became asymmetric; the maximum charge displaced in the on-gating current remained unchanged at about 1 nC (Figure 5C, squares), whereas that in the off-gating current increased to 3 nC (Figure 5B, squares).

Since gating charge displacement in the on-gating currents reflects the charged state of the His-365 residue at the starting potential of −130 mV, it should be independent of external pH for all test pulses. However, while the maximum on-gating charge displacement remained the same in external pH 9.2 and 5, both the voltage dependence and the shape of the on-gating Q-V curves changed (Figure 5C). The shift of the Q-V curve to more depolarized potentials with decreasing external pH arises, most likely, from a screening of fixed charges by external protons (see Hille, 1992), a phenomenon also observed in control channels without the His-365 replacement (data not shown). The Q-V curve for on-gating in external pH 5 (Figure 5C, triangles and squares) has a region with a nonmonotonic increase (Figure 5C, triangles) that encompasses the voltage region of large proton transport (Figures 2B and 3A). This proton current makes estimation of the gating charge unreliable but does not affect the gating charge measurements at extreme potentials where the proton current is negligible (Figure 5C, squares). Therefore, the differences in the shape and voltage dependence of the on-gating Q-V curves shown in Figure 5C are not due to an effect of the external pH on the charge of the His-365 residue in the hyperpolarized state. The maximum on-gating charge displacement should be unaffected by surface charge screening and the proton current, and it is indeed independent of external pH.

The Q-V curve for off-gating indicates that His-365 was fully protonated at pH 5 since the increase of maximum charge displacement with decreasing pH saturated by pH 5 (Figure 5B). If we assume that gating charge motion in the fully protonated form of the R365H channel is the same as in the wild-type channel, then at pH 5, a maximum of 12–13 e_0 per channel (Q/N) traverses the electric field during gating (Schoppa et al., 1992). This assumption allows estimation of the maximum off-charge per channel (Q_{off}/N) in each external pH (Figure 5B). At pH 9.2, the gating charge displacement was reduced by 8–9 e_0 per channel. The modulation of gating charge displacement by extracellular protons fit a two-state model with a pK_a of 7.6, indicative of titration of the histidine (Figure 5D). Although the pK_a of histidine in solution is 6.0, environment-dependent pK_a shifts of amino acid residues are quite common, and for histidine, it can range from 5.4 to 8 (Cohen et al., 1970; Rüterjans and Pongs, 1971); in the *Shaker* K^+ channel, for example, a histidine replacing a residue in the pore had a reported pK_a of 7.7 (Lu and MacKinnon, 1995).

Discussion

A Model of Proton Transport by a Titratable Voltage Sensor

Gating currents can be thought of as charge-carrying transitions among states connected by voltage-dependent rate constants. A gating current, then, is the physical manifestation of a change in the population of a charged state with time. A simple model of a voltage sensor with a protonatable residue is shown in Figure 6. The voltage sensor can occupy states exposed to the extracellular (**D**) or intracellular (**H**) solution. The transitions between **D** and **H** are driven by voltage, since the rate constants α_1, α_2, β_1, and β_2 are voltage-dependent. In general, α_n approaches zero at very negative potential differences and β_n approaches zero at very large potential differences, so that hyperpolarization of the positively charged voltage sensor favors occupation of **H** states and depolarization favors occupation of **D** states. On each side of the membrane, the voltage sensor can exist in an unprotonated state (I, internal and E, external) with charge z or a protonated state (IH^+ or EH^+) with

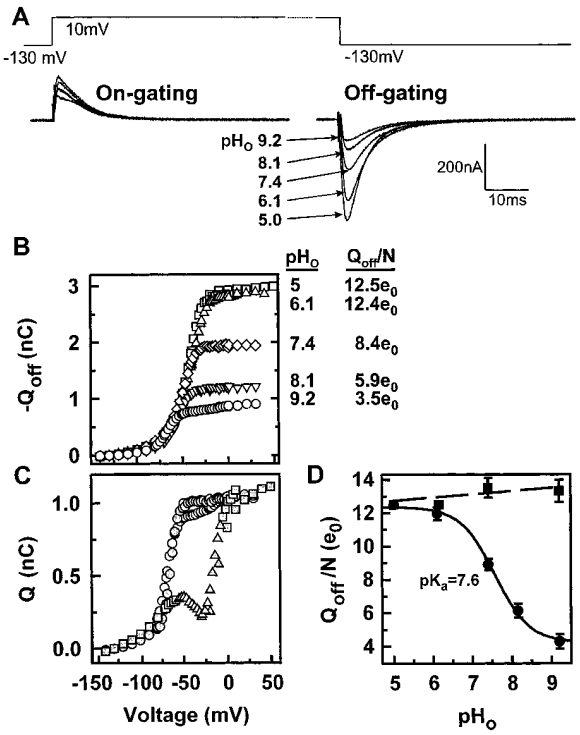

Figure 5. Titration of Gating Charge Displacement with External Protons in the R365H Channel

On- and off-gating currents were measured in pH 9.2 internal solution and several external pHs (pH_o) from the same oocyte. The initial and final solution conditions were symmetric pH 9.2, and the measurements from the two sets were averaged to accommodate the small rundown of channels during the experiment.

(A) On- and off-gating currents measured in each pH_o, in response to a test pulse to 10 mV. Although the on-gating currents appear different, changes in amplitude are almost completely compensated by changes in kinetics so that the on-charge displaced, Q, is approximately equal in all pH_os.

(B) Q-V curves from off-gating currents measured in pH_o 9.2 (circles), 8.1 (inverted triangles), 7.4 (diamonds), 6.1 (triangles), or 5 (squares). Total gating charge per channel, (Q_{off}/N), was estimated by assuming that it is 12.5 e_0 at pH_o 5.

(C) Q-V curves from on-gating currents measured in pH_o 9.2 (closed circles) and 5 (closed squares and triangles) (the currents are shown in Figures 2A and 2B). For comparison, the Q-V curve for the off-gating currents, measured in pH_o 9.2 (open circles), is also shown.

(D) The dependence of Q_{off}/N on pH_o for the R365H channel (circles) and the control, H4IR[W434F] (squares). Each point is the mean ± SEM of 3–11 measurements from separate oocytes. The curve through the circles is a best fit to the Henderson-Hasselbach equation: $Q_{off}/N = Min + ([Max - Min]/[1 + \exp\{2.3026(pH_o - pK_a)\}])$ The fit gives a pK_a of 7.6. The dashed line through the squares is a linear regression.

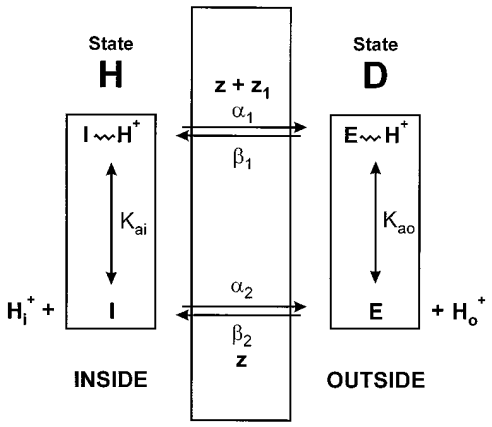

Figure 6. A Model of the Gating Charge Transitions for a Voltage Sensor with a Histidine

The charge carried by the voltage sensor z or $z + z_1$ is dependent on the charged state of a protonatable residue, such as histidine. K_a is the equilibrium constant between the protonated and unprotonated form of His. Since the S4 segment, which contains most of the voltage-sensing residues, is positively charged, a depolarization of the membrane (gray box) moves the voltage sensor from the inside of the membrane toward the outside, thereby moving the gating charge z or $z + z_1$ in the transition. Similarly, repolarization results in a charge-carrying transition to a state closer to the inside. The transition rates α and β incorporate the voltage dependence. Therefore, if the His residue of the voltage sensor is exposed to the surrounding solution in a particular state, then the charge carried during gating transitions will be dependent on the pH of the surrounding solution.

charge $z + z_1$. The equilibrium between protonated and unprotonated states is dependent on the pK_a of the titratable residue and the pH of the surrounding solvent. We assume that the states on each side of the membrane reach equilibrium infinitely fast since the rate constants for protonation and deprotonation of a histidine residue (Eigen et al., 1960; Kasianowicz et al., 1987) are a few orders of magnitude greater than those for gating transitions between hyperpolarized and depolarized states (Bezanilla et al., 1994). Then, states **D** and **H** each consist of an equilibrium mixture of states; f_i, the fraction of internally exposed voltage sensors in the protonated state, can be expressed as

$$f_i = \frac{[IH^+]}{[IH^+] + [I]} = \frac{[H_i^+]}{[H_i^+] + K_{ai}} = \frac{1}{1 + \exp[2.3(pH_i - pK_{ai})]},$$

and f_o, the fraction of externally exposed voltage sensors in the protonated state, is

$$f_o = \frac{[EH^+]}{[EH^+] + [E]} = \frac{[H_o^+]}{[H_o^+] + K_{ao}} = \frac{1}{1 + \exp[2.3(pH_o - pK_{ao})]}.$$

The transitions of the voltage sensor between states **D** and **H** move charge z or $z + z_1$ across the transmembrane electric field and thereby generate a gating current. No current will arise from transitions between protonated and unprotonated states since there is no potential difference between them. The derivation of an expression for the gating currents predicted by the model is given in the Appendix. For N channels, the on-gating current i_g, produced upon depolarization from an extremely hyperpolarized initial state (**D**(t=0) = 0 and **H**(t=0) = 1) to various test potentials V, contains a transient, exponentially decaying component and a steady component given by

$$i_g(t,V) = \frac{N\alpha'}{\alpha' + \beta'}[z(\alpha' + \beta') + z_1(\alpha_1 f_i + \beta_1 f_o)]e^{-(\alpha' + \beta')t} +$$

$$\frac{Nz_1(\alpha_1\beta' f_i - \alpha'\beta_1 f_o)}{\alpha' + \beta'}$$

where α' and β' are composite forward and backward rate constants (see Appendix, equation A2). The steady component of the gating current is a constant proton current that carries the excess charge, z_1, transported by the titratable residue. It is driven by both the transmembrane potential and pH gradient. At very hyperpolarized or depolarized potentials, where α or β approaches zero and the voltage sensor is driven to remain most of the time in either the **H** or **D** state, the proton current goes to zero. Indeed, with the very hyperpolarized return potentials used to elicit off-gating currents experimentally, a constant proton current is neither predicted (see Appendix, equation A6) nor observed. As the forward and backward rate constants converge and the voltage sensor makes increasingly frequent transitions between **H** and **D** states, the proton current grows.

In order to examine the voltage dependence of the proton current more closely, the simple case of a very large pH gradient will be considered. For example, when the internal pH is very high, all voltage sensors in **H** states will be unprotonated ($f_i = 0$); when the external pH is very small, all voltage sensors in **D** states will be protonated ($f_o = 1$). Then the transitions between **H** and **D** will proceed via the α_2 and β_1 loop (Figure 6). In this extremely large transmembrane pH gradient, the on-gating current has a simple form:

$$i_g = \frac{N\alpha_2[z\alpha_2 + (z + z_1)\beta_1]}{\alpha_2 + \beta_1} e^{-(\alpha_2 + \beta_1)t} - \frac{Nz_1\alpha_2\beta_1}{\alpha_2 + \beta_1}. \quad (1)$$

The direction of the steady proton current is inward since protons are transported from the acidic external solution to the basic internal solution. Clearly, the steady proton current goes to zero at very hyperpolarized or depolarized potentials as either of the rate constants approaches zero. The maximum inward proton current, obtained using the general form of the rate constants given in the Appendix (equation A4), occurs at the potential where $q_{\alpha 1}\beta_2 = q_{\beta 2}\alpha_1$. The fractional charge q determines the steepness of the voltage dependence of the rate constants; it is the product of the charge and the fraction of the transmembrane electric field that the charge must traverse to hurdle the energy barrier of the state. Therefore, the potential of peak proton transport is slightly shifted from the potential of half-maximal gating charge displacement, and the shift is determined by the steepness of the voltage dependence of the rate constants.

For the general case in which the voltage sensor is partially protonated on each side of the membrane and all rate constants are involved, maximum proton transport has a more complicated relationship to the voltage dependence of all four rate constants and to the transmembrane pH gradient. This is consistent with the shift of transport observed in Figure 4B. Moreover, the asymmetry of the voltage dependence of proton conductance, observed in some experimental conditions, is qualitatively consistent with a difference in the voltage dependence of forward and backward rate constants.

The Rate of Proton Transport

The rate of proton transport per channel can be estimated from the rate constant of the decay of the transient component of the gating current. For the simple case of a large pH gradient, the transient component decays with a rate constant of approximately $2\alpha_1$ when the steady proton current is maximal (equation 1 with $\alpha_2 = \beta_1$). Since it was shown that the His-365 residue was fully protonated at pH 5 and unprotonated at pH 9.2 (Figure 5B), application of external pH 5 and internal pH 9.2 supplies a pH gradient large enough to apply our simple case to the data. The decay of R365H channel gating currents, measured at room temperature in response to test pulses that generated maximum proton current ($pH_i - pH_o = 4.2$), were fit to decaying exponential functions of the form

$$A\exp(-2\alpha_2 t) + B$$

where A and B are constants. Although the gating current kinetics at the potential of maximum steady current have a rising phase and at least two decaying exponentials, the fit was reasonably approximated by a single exponential decay. The average rate of maximum proton transport α_1 obtained from the fits was 178 ± 13 s^{-1} (± SEM; n = 7). This rate is comparable to other known proton transporters, which range from 25–100 s^{-1} (Boorer et al., 1996).

The rate of transport can also be determined directly from the maximum proton current measured. According to equation 1, the rate of maximum proton transport in a large pH gradient is approximately

$$\alpha_1 = 2\frac{I_{pMax}}{Nz_1}$$

Peak proton currents, I_{pMax}, were measured in external pH 5 and internal pH 9.2; the number of channels, N, was estimated by assuming that in pH 5, when the externally exposed His-365 residue is fully protonated, the maximum measured off-gating charge displaced was 12.5 e_0 per channel, as in the wild-type channel (Schoppa et al., 1992). According to the model, four fully protonated histidine residues move across the whole membrane field during transport by the tetrameric K^+ channel ($z_1 = 4\ e_0$). With a transport of 4 e_0, the average transport rate α_1 obtained from the measurements of I_{pMax} was 177 ± 17 s^{-1} (± SEM; n = 7), in excellent agreement with the rate obtained from the decay of the transient gating current. This agreement between the model and the data implies that the His-365 residue of all four subunits of the channel oscillates between internal and external exposure, and the rates of protonation and deprotonation of the residue are not rate-limiting.

The movement of four charges across the entire membrane field, deduced from the measurement of R365H proton transport rates, contrasts with the decrease of 8.2 ± 0.4 e_0 (± SEM) with deprotonation of His-365, deduced from the measurements of gating charge displacement. However, gating charge displacement is a

measurement of the product of the charge and the fraction of electric field it traverses; the two quantities cannot be experimentally discerned with gating current measurements. Therefore, determination of the gating charge displacement of the R365H channel measures not only the charge contribution of residue 365 to gating but also the effect of the His substitution on the charge displacement of the other residues. Since the data discussed above indicates that His-365 traverses the entire field during gating and can transport four charges per channel, the replacement of Arg-365 with a histidine in its protonated form probably does not affect the transmembrane electric field or the movement of unmutated residues. If so, the extra 4.2 e_0 removed by His-365 in measurements of gating charge displacement may be due to the influence of the unprotonated form of His-365 on the electric field and on the movement of unmutated residues; by extending the region of protein that the electric field spans, the product of other gating charges and the fraction of field they traverse could be substantially decreased. There is previous evidence for such interactions between gating charge and the electric field since a decrease of much more than four gating charges per channel has been reported when other voltage-sensing charges were removed (Seoh et al., 1996). The ability to measure the actual gating charge in transport as well as its influence on the electric field in the charge displacement of other residues provides a unique opportunity to examine the local electric field. However, such an analysis must be made with caution, especially since the transmembrane electric field may extend a small distance into narrow, hydrophilic crevices that penetrate the protein.

The simplest model of a titratable voltage sensor predicts behavior that qualitatively agrees with the observed behavior of the R365H and R368H channels. This agreement lends substantial support to the coupling of gating and proton transport by the His residue and provides a theoretical framework to understand the phenomenon. Since only four states in the proton transport were experimentally distinguishable, nothing would be gained with a more complex model. However, the *Shaker* K^+ channel requires a model with many more states to account for all details of the gating currents quantitatively (Bezanilla et al., 1994).

The Environment of Voltage-Sensing Residues, R365 and R368

This is a novel demonstration of internal access to residue 365 and external access to residue 368. Failure to detect it previously using various cysteine probes (Larsson et al., 1996; Yusaf et al., 1996) indicates that the hydrophilic passages to residues 365 and 368 are too confined for the entrance of these probes. M. Holmgren and G. Yellen were able to access R365C internally with MTSET only when extremely hyperpolarized potentials were applied. The reaction was very slow, consistent with the idea that residue 365 is confined to a narrow hydrophilic crevice (personal communication). Earlier work identifying the charge contribution and solvent accessibilities of specific residues during gating charge displacement has defined an outermost boundary of a small region of the S4 segment in which the electric field is focused (Yang and Horn, 1995; Aggarwal and MacKinnon, 1996; Larsson et al., 1996; Seoh et al., 1996; Yang et al., 1996; Yusaf et al., 1996). The use of protons to titrate histidine-substituted residues probes the environment with higher resolution and less interference than the larger sulfhydryl-specific labels frequently used.

Conclusions

Probing the boundary of the electric field with protons indicates that the voltage-sensing residue 365 lies on an internally faced narrow crevice in the resting state, while the sensing charge at position 368 sits in an externally faced crevice in the open state of the channel. Both residues move entirely from the internal to external medium in each stroke of the voltage sensor, which relaxes the requirement for counter charges in other transmembrane segments. Moreover, the translocation of these two residues accounts for 66% of the total gating charge and could therefore carry most of the elementary shot of 2.4 e_0 measured by noise analysis of gating currents (Sigg et al., 1994). The hydrophilic crevices that penetrate the hydrophobic environment of the protein focus the transmembrane electric field in a narrow voltage-sensitive region of the S4 segment. This specialized structure enables small conformational changes to accomplish the work of moving charges across the entire transmembrane electric field.

The method of site-directed His mutagenesis has also revealed a novel mechanism of proton transport regulated by both the transmembrane electric field and the transmembrane pH gradient. The bell-shaped voltage dependence of the proton transport is a special case that occurs in a large pH gradient when the forward rate constants (α_1, α_2) increase with voltage and the backward rate constants (β_1, β_2) decrease with voltage. A sigmoidal voltage dependence (a common case in experimentally observed proton conductances) would be obtained if the forward rates increased with voltage and the backward rates were constant. Although the histidine-substituted *Shaker* K^+ channel is an artificial transporter, it is conceivable that the mechanism of proton transport reported here could be found in wild-type cells to regulate the intracellular and intraorganelle pH with the membrane potential.

Experimental Procedures

Mutagenesis and Expression of Channels

Mutation of the arginine at position 365 or 368 to a histidine was generated by PCR with mutagenic primers that replaced the codon CGA with CAC (Ho et al., 1989). The template for mutagenesis was a modified version of the nonconducting (W434F) (Perozo et al., 1993), noninactivating (Δ6–46) (Hoshi et al., 1990) *Shaker* K^+ channel cDNA (Schwarz et al., 1988), cloned into the vector pBSTA (kindly provided by A. Goldin) (Liman et al., 1992; Shih and Goldin, 1997). The *Shaker* K^+ channel cDNA was modified to increase expression by removing the 5′ and 3′ untranslated regions and inserting the Kozak consensus sequence GCCACC immediately upstream of the starting ATG codon (Kozak, 1991). The mutagenic fragment generated by PCR was sequenced. To express the channel, cRNA was synthesized from the NotI-linearized DNA clone (New England Biolabs) with T7 RNA polymerase (Ambion mMessage mMachine *In*

Vitro Transcription Kit), and 2 nl of 0.8 μg/μl cRNA was injected into each prepared stage 5 Xenopus oocyte (Timpe et al., 1988).

Electrophysiological Recordings

All gating currents were measured with the cut-open oocyte voltage-clamp technique (Stefani et al., 1994) 3–6 days after injection of oocytes. The external solution contained 120 mM n-methylglucamine (NMG), 2 mM $CaCl_2$, and 10 mM buffer titrated to the appropriate pH with methanesulfonic acid (MES); for pH 9.2 solutions, the buffer used was 2-(N- cyclohexylamino)ethanesulfonic acid (CHES), and for all other pHs, it was HEPES. The internal solution was the same as the external except that $CaCl_2$ was replaced with EGTA-NMG. Data was filtered at 2–2.5 kHz with a 6-pole Bessel filter in series with the 4-pole filter of the amplifier set at 100 kHz and was digitized with our own interface at a frequency five times greater than the filter frequency. From a holding potential of −90 mV, currents were measured in response to various test pulses preceded and followed by a pulse to −130 mV. Test pulses were at least 100 ms long and were made at least 2 s apart. Linear membrane capacitance was compensated electronically at 0 mV, and no pulse subtraction protocol was used. Only those experiments that were reversible with respect to the effect of pH are reported. Unless otherwise indicated, all experiments were done at 19°C–21°C.

Appendix

A Model of Proton Transport by the Voltage Sensor

A simple model of the states that the voltage sensor can occupy is shown in Figure 6. A gating current will be produced with charge carrying transitions from states on one side of the membrane to states on the opposite side. Then, a gating current will be produced by a change with time in the population of all externally exposed states, **D**, or all internally exposed states, **H**. The change in the probability of occupying states in **D** is given by:

$$\frac{d\boldsymbol{D}}{dt} = (\alpha_1[I\boldsymbol{H}^+] + \alpha_2[\boldsymbol{I}]) - (\beta_1[\boldsymbol{E}\boldsymbol{H}^+] + \beta_2[\boldsymbol{E}]) , \qquad \text{(A1)}$$

where the square brackets denote relative concentrations or probabilities

$$[I\boldsymbol{H}^+] + [\boldsymbol{I}] + [\boldsymbol{E}\boldsymbol{H}^+] + [\boldsymbol{E}] = 1$$

and

$$[I\boldsymbol{H}^+] + [\boldsymbol{I}] = \boldsymbol{H} \qquad [\boldsymbol{E}\boldsymbol{H}^+] + [\boldsymbol{E}] = \boldsymbol{D} .$$

The dissociation constants K_{ai} and K_{ao} determine the relative occupancy of protonated and unprotonated states on each side of the membrane.

$$K_{ai} = \frac{[\boldsymbol{I}]\,[H_i^+]}{[I\boldsymbol{H}^+]} \qquad K_{ao} = \frac{[\boldsymbol{E}]\,[H_o^+]}{[\boldsymbol{E}\boldsymbol{H}^+]} .$$

We assume that the states on each side of the membrane, E and EH^+ or I and IH^+, reach equilibrium infinitely fast since the rate constants for protonation and deprotonation of a His residue (Eigen et al., 1960; Kasianowicz et al., 1987) are a few orders of magnitude greater than those for gating transitions between hyperpolarized and depolarized states. Then, f_i, the fraction of internally exposed voltage sensors in the protonated state, can be expressed as

$$f_i = \frac{[I\boldsymbol{H}^+]}{[I\boldsymbol{H}^+] + [\boldsymbol{I}]} = \frac{[H_i^+]}{[H_i^+] + K_{ai}} , =$$

$$\frac{1}{1 + \exp[2.3(pH_i - pK_{ai})]} ,$$

and f_o, the fraction of externally exposed voltage sensors in the protonated state, is

$$f_o = \frac{[\boldsymbol{E}\boldsymbol{H}^+]}{[\boldsymbol{E}\boldsymbol{H}^+] + [\boldsymbol{E}]} = \frac{[H_o^+]}{[H_o^+] + K_{ao}} =$$

$$\frac{1}{1 + \exp[2.3(pH_o - pK_{ao})]} .$$

Substitution of f_i, f_o, **H**, and **D** into equation A1 yields the differential equation

$$\frac{d\boldsymbol{D}}{dt} = \boldsymbol{H}[\alpha_1 f_i + \alpha_2(1 - f_i)] - \boldsymbol{D}[\beta_1 f_o + \beta_2(1 - f_o)] =$$

$$-\boldsymbol{D}(\alpha' + \beta') + \alpha' ,$$

where α' and β' are composite rate constants given by

$$\alpha' = \alpha_1 f_i + \alpha_2(1 - f_i) \qquad \beta' = \beta_1 f_o + \beta_2(1 - f_o) . \qquad \text{(A2)}$$

The solution to the differential equation gives the occupancy of **D** as a function of time, t, and voltage, V.

$$\boldsymbol{D}(t,V) = (\boldsymbol{D_0} - \boldsymbol{D}_\infty)e^{-(\alpha' + \beta')t} + \boldsymbol{D}_\infty = 1 - \boldsymbol{H}(t,V) , \qquad \text{(A3)}$$

where $\mathbf{D_0}$ is the occupancy evaluated at t = 0 and $\mathbf{D}_\infty$ is the value as $t \rightarrow \infty$:

$$\boldsymbol{D_0} = \boldsymbol{D}(t = 0,\, V = V_0) = \frac{\alpha'_{V_0}}{\alpha'_{V_0} + \beta'_{V_0}}$$

$$\boldsymbol{D}_\infty = \boldsymbol{D}(t \rightarrow \infty,\, V) = \frac{\alpha'}{\alpha' + \beta'} .$$

The voltage dependence of transitions between **D** and **H** states is determined by the rate constants α_1, α_2, β_1, and β_2 such that, at equilibrium, the relative occupancy of each state, as a function of voltage, follows a Boltzmann distribution. The electrical energy of each state is a product of the potential difference across the membrane, V, the charge of the state, z or $z + z_1$, and the fraction of the transmembrane field that the charge traverses to overcome the energy barrier separating the states. A change in protonation affects not only the state charge but also the electric field and thereby the fractional distance that the charge must traverse to escape the state. Therefore, a general form of the rate constants is given in terms of the fractional charge, q, a product of the charge and the fraction of the field it traverses:

$$\alpha_n = \alpha_0 \exp[q_{\alpha_n} V/kT]$$

$$\beta_n = \beta_0 \exp[-q_{\beta_n} V/kT] . \qquad \text{(A4)}$$

α_0 and β_0 are conformational energy terms, k is Boltzmann's constant, and T is the temperature. In general, α_n approaches zero at very negative potential differences and β_n approaches zero at very large potential differences, so that hyperpolarization of the positively charged voltage sensor favors occupation of **H** states and depolarization favors occupation of **D** states.

The requirement of microscopic reversibility imposes constraints on the relationship between the transition rate constants. In the case where the pH on each side of the membrane is the same ($[H_i^+] = [H_o^+]$), microscopic reversibility is satisfied if there is no net proton circulation across the membrane and

$$\alpha_1\beta_2 K_{ai} = \alpha_2\beta_1 K_{ao} .$$

The transitions of the voltage sensor between states **D** and **H** move charge z or $z + z_1$ across the transmembrane electric field and thereby generate a current, i_g. For N channels, the on current predicted by the model is

$$i_g = N(\boldsymbol{H}[\{z + z_1\}\alpha_1 f_i + z\alpha_2\{1 - f_i\}] - \boldsymbol{D}[\{z + z_1\}\beta_1 f_o + z\beta_2\{1 - f_o\}]) .$$

A general expression for the on-gating current, obtained by substitution of the explicit equation for **D** (equation A3) is given below:

$$i_g = N[\frac{\alpha'}{\alpha' + \beta'} - \boldsymbol{D_0}][z(\alpha' + \beta') + z_1(\alpha_1 f_i + \beta_1 f_o)]e^{-(\alpha' + \beta')t} +$$

$$\frac{Nz_1(\alpha_1\beta' f_i - \alpha'\beta_1 f_o)}{\alpha' + \beta'} . \qquad \text{(A5)}$$

All rate constants, except α_{V0}' and β_{V0}', are evaluated at the potential of the test pulse V; α_{V0}' and β_{V0}' are evaluated at the initial prepulse potential, V_0. The second term of the on-gating current is a steady proton current proportional to the charge z_1. In a large transmembrane pH gradient, if $q_\alpha > 0$ and $q_\beta > 0$ (if the rate constants are

voltage-dependent, see equation A4), the proton current will have a bell-shaped voltage dependence and will vanish at $V \rightarrow \pm\infty$, as we have observed experimentally. However, when either $q_\alpha = 0$ or $q_\beta = 0$ (when one of the rate constants is not voltage-dependent), the proton current will exhibit sigmoidal voltage dependence.

For the very hyperpolarized prepulses (−130 mV) used in the experiments described here, $\mathbf{D_0}$ approaches zero and the predicted on-gating current is

$$i_g(t,V) = \frac{N\alpha'}{\alpha' + \beta'}\,[z(\alpha' + \beta') + z_1(\alpha_1 f_i + \beta_1 f_o)]e^{-(\alpha' + \beta')t} + \frac{Nz_1(\alpha_1\beta' f_i - \alpha'\beta_1 f_o)}{\alpha' + \beta'}.$$

The expression for the off-gating current is equal and opposite to that for the on-gating current (equation A5). However, all rate constants except α_{v0}' and β_{v0}' are evaluated at the potential of the postpulse; α_{v0}' and β_{v0}' are evaluated at the test pulse potential. For the very hyperpolarized postpulses (−130 mV) used in the experiments, α_1, α_2, and $\mathbf{D}_\infty$ approach zero and

$$i_{g(OFF)}(t,V \rightarrow -\infty) = \frac{N\alpha_{V_0}}{\alpha_{V_0} + \beta_{V_0}}(z\beta' + z_1\beta_1 f_0)e^{-\beta' t}. \qquad \text{(A6)}$$

Acknowledgments

We thank Dr. Adrian Gross, Daniel Sigg, and all members of the Bezanilla laboratory for their comments on the manuscript and many helpful discussions. This work was supported by National Institutes of Health grant GM30376.

Received September 2, 1997; revised October 13, 1997.

References

Aggarwal, S.K., and MacKinnon, R. (1996). Contribution of the S4 segment to gating charge in the *Shaker* K^+ channel. Neuron *16*, 1169–1177.

Armstrong, C.M., and Bezanilla, F. (1973). Currents related to movement of the gating particles of the sodium channels. Nature *242*, 459–461.

Bezanilla, F., Perozo, E., and Stefani, E. (1994). Gating of *Shaker* K^+ channels: II. The components of gating currents and a model of channel activation. Biophys. J. *66*, 1011–1021.

Boorer, K.J., Frommer, W.B., Bush, D.R., Kreman, M., Loo, D.D.F., and Wright, E.M. (1996). Kinetics and specificity of a H^+/amino acid transporter from *Arabidopsis thaliana*. J. Biol. Chem. *271*, 2213–2220.

Cohen, J.S., Shrager, R., McNeel, M., and Schnechter, A.N. (1970). On-line computer-assisted analysis of 220mhz NMR data of protein imidazole resonances. Biochim. Biophys. Acta *40*, 144–151.

Eigen, M., Hammes, G.G., and Kustin, K. (1960). Fast reactions of imidazole studied with relaxation spectrometry. J. Am. Chem. Soc. *82*, 3482–3483.

Hille, B. (1992). Modifiers of gating. In Ionic Channels of Excitable Membranes, 2nd Ed. (Sunderland, MA: Sinauer Associates Inc.), pp. 458–467.

Ho, S.N., Hunt, H.D., Horton, R.M., Pullen, J.K., and Pease, L.R. (1989). Site-directed mutagenesis by overlap extension using the polymerase chain reaction. Gene *77*, 51–59.

Hodgkin, A.L., and Huxley, A.F. (1952). A quantitative description of membrane current and its application to conduction and excitation in nerve. J. Physiol. *117*, 500–544.

Hoshi, T., Zagotta, W.N., and Aldrich, R.W. (1990). Biophysical and molecular mechanisms of *Shaker* potassium channel inactivation. Science *250*, 533–538.

Kasianowicz, J., Benz, R., and McLaughlin, S. (1987). How do protons cross the membrane-solution interface? Kinetic studies on bilayer membranes exposed to protonophore S-13 (5-chloro-3-tert-butyl-2'-chloro-4' nitrosalicylanilide). J. Mem. Biol. *95*, 73–89.

Kozak, M. (1991). Structural features in eukaryotic mRNAs that modulate the initiation of translation. J. Biol. Chem. *266*, 19867–19870.

Larsson, H.P., Baker, O.S., Dhillon, D.S., and Isacoff, E.Y. (1996). Transmembrane movement of the *Shaker* K^+ channel S4. Neuron *16*, 387–397.

Liman, E.R., Tytgat, J., and Hess, P. (1992). Subunit stoichiometry of a mammalian K^+ channel determined by construction of multimeric cDNAs. Neuron *9*, 861–871.

Lu, Z., and MacKinnon, R. (1995). Probing a potassium channel pore with an engineered protonatable site. Biochemistry *34*, 13133–13138.

MacKinnon, R. (1991). Determination of the subunit stoichiometry of a voltage-activated potassium channel. Nature *350*, 232–235.

Perozo, E., MacKinnon, R., Bezanilla, F., and Stefani, E. (1993). Gating currents from a nonconducting mutant reveal open-closed conformations in *Shaker* K^+ channels. Neuron *11*, 353–358.

Rodriguez, B.M., Sigg, D., and Bezanilla, F. (1995). Temperature dependence of gating current (I_g) in *Shaker* B K^+-channel. Biophys. J. *68*, A137.

Rüterjans, H., and Pongs, O. (1971). On the mechanism of action of ribonuclease T1 nuclear magnetic resonance study on the actice site. Eur. J. Biochem. *18*, 313–318.

Schoppa, N.E., McCormack, K., Tanouye, M.A., and Sigworth, F.J. (1992). The size of gating charge in wild-type and mutant *Shaker* potassium channels. Science *255*, 1712–1715.

Schwarz, T.L., Tempel, B.L., Papazian, D.M., Jan, Y.N., and Jan, L.Y. (1988). Multiple potassium-channel components are produced by alternative splicing at the Shaker locus in *Drosophila*. Nature *331*, 137–142.

Seoh, S.-A., Sigg, D., Papazian, D.M., and Bezanilla, F. (1996). Voltage-sensing residues in the S2 and S4 segments of the *Shaker* K^+ channel. Neuron *16*, 1159–1167.

Shih, T.M., and Goldin, A.L. (1997). Topology of the *Shaker* potassium channel probed with hydrophilic epitope insertions. J. Cell Biol. *136*, 1037–1045.

Sigg, D., Stefani, E., and Bezanilla, F. (1994). Gating current noise produced by elementary transitions in *Shaker* potassium channels. Science *264*, 578–582.

Stefani, E., Toro, L., Perozo, E., and Bezanilla, F. (1994). Gating of *Shaker* K^+ channels: I. Ionic and gating currents. Biophys. J. *66*, 996–1010.

Timpe, L.C., Schwarz, T.L., Tempel, B.L., Papazian, D.M., Jan, Y.N., and Jan, L.Y. (1988). Expression of functional potassium channels from *Shaker* cDNA in *Xenopus* oocytes. Nature *331*, 143–145.

Yang, N., and Horn, R. (1995). Evidence for voltage-dependent S4 movement in sodium channels. Neuron *15*, 213–218.

Yang, N., George, A.L., Jr., and Horn, R. (1996). Molecular basis of charge movement in voltage-gated sodium channels. Neuron *16*, 113–122.

Yusaf, S.P., Wray, D., and Sivaprasadarao, A. (1996). Measurement of the movement of the S4 segment during the activation of a voltage-gated potassium channel. Pflügers Arch. *433*, 91–97.